

Formation and Evolution of sub-structures in tidal tails: Spherical dark matter haloes

B. Reinoso^{1*}, M. Fellhauer^{1†}, R. Véjar¹

¹*Departamento de Astronomía, Universidad de Concepción, Casilla 160-C, Concepción, Chile*

28 October 2021

ABSTRACT

Recently a theory about the formation of over-densities of stars along tidal tails of globular clusters has been presented, this theory predicts the position and time of formation of such over-densities and was successfully tested with N-body simulations of globular clusters in a point mass galactic potential. In this work we present a comparison between this theory and our simulations using a dwarf galaxy orbiting two differently shaped dark matter halos to study the effects of a cored and a cuspy halo on the formation and evolution of tidal tails. We find no difference using a cuspy or a cored halo, however, we find an intriguing asymmetry between the leading and trailing arm of the tidal tails. The trailing arm grows faster than the leading arm. This asymmetry is seen in the distance to first over-density and its size as well. We establish a relation between the distance to the first over-density and the size of this over-density.

Key words: methods: numerical — galaxies: dwarfs — galaxies: kinematics and dynamics — galaxies: structures — galaxies: haloes

1 INTRODUCTION

An image of the globular cluster Palomar 5 (Pal 5) and its tidal tails has been published by Odenkirchen et al. (2001). In this image the tidal tails of Pal 5 along with some over-densities within them are clearly visible. Besides Pal 5, there are also other satellites of the Milky Way (MW) which have elongated structures, for example the Sagittarius (Sgr) dwarf spheroidal galaxy (dSph), whose tidal tails were described by Majewski et al. (2003), the Virgo stellar stream (Vivas et al. 2001) the new Aquarius stream (Williams et al. 2011) and all the streams listed in the Field of Streams (Belokurov et al. 2006).

Tidal tails could be useful to constrain the properties of the Milky Way (MW) like the mass and the shape of the dark matter (DM) halo. Koposov et al. (2010), using a 6D space map of the GD-1 stream in Andromeda, found that an eccentric orbit in a flattened isothermal potential ($q_{\Phi} = 0.87_{-0.04}^{+0.07}$) fits the parameters of distance, line-of-sight velocity and proper motion of the stars in the stream. Fellhauer et al. (2006) demonstrated that if the tails of the Sagittarius dSph are wrapping around twice the MW, causing the visible bifurcation (Belokurov et al. 2006), then the MW DM halo has to be close to spherical.

To recover the Galactic potential using tidal tails, the

first step is to determine the orbit of the satellite by looking at the elongation of its tails. The next step is to perform simulations using different Galactic potentials and assuming properties of the satellite like the initial mass, the eccentricity of the orbit or the distance to its apo-centre or peri-centre. Finally, one has to compare the final properties of the stars in the debris like the velocity dispersion, line of sight velocity and proper motion with data from observations. The bias from this method comes from the fact that one has to assume properties of the satellite and/or the Milky Way. However, the study of the formation of tidal tails could give us some clues about the initial properties of the disrupting satellites, thus improving the methods to constrain Galactic properties.

Following this line, Küpper et al. (2008) published a theory which explains how tidal tails are formed. In their work, they propose that the stars that escape from a globular cluster move in epicycles inside a galactic potential. They found good agreement between their theory and N-body simulations of globular clusters under the influence of a point mass galaxy (Küpper et al. 2008, 2010, 2012).

In their theory, Küpper et al. (2008) make the approach that all the particles escaping from the satellite have small velocities with respect to the satellite and they escape always through the Lagrangian points L1 and L2, therefore two symmetrical tails are formed, a leading arm where particles orbit ahead of the satellite and a trailing arm where particles orbit behind the satellite. With these assumptions

* E-mail: breinoso@udec.cl

† E-mail: mfellhauer@astro-udec.cl

they derive equations which predict the position and time of formation of over-densities along both tails assuming that if D is the distance to the first over-density in the leading arm, then $-D$ is the distance to the first over-density in the trailing arm where the reference frame is in the centre of the satellite.

Our goal is to check the theory of Küpper et al. (2008) comparing their predictions with simulations performed by SUPERBOX (a collision-less particle mesh code; see Fellhauer et al. 2000) using a dwarf satellite and modeling the Milky Way dark matter halo either with a logarithmic halo (cored profile) or with a Navarro-Frenk-White (NFW) halo (cuspy profile Navarro et al. 1996).

The paper is organized as follows: In Section 2 we describe the properties of the satellites used in our simulations, the dark matter potential and the orbits of the satellites. In Section 3 we describe the analysis of the data and how we estimate our errors. In Section 4 we present our results. In Section 5 we discuss the results and present our conclusions.

2 SETUP

To integrate the particles forward in time, we use SUPERBOX (Fellhauer et al. 2000), a collision-less particle mesh code which uses 3 levels of grids, with the two high-resolution grids staying focused on the simulated and moving object. This makes the code faster by improving resolution only at the places of interest.

To model the MW DM halo we use analytic potentials. For the cored case we use a logarithmic potential given by:

$$\Phi = \frac{1}{2}v_c^2 \ln(r^2 + d^2), \quad (1)$$

where r is the distance to the centre of the galaxy, $v_c = 220 \text{ km s}^{-1}$ and $d = 12 \text{ kpc}$.

Alternatively, to mimic a cusped potential, we use a Navarro-Frenk-White potential:

$$\Phi = 4\pi G\rho_0 \frac{r_s^3}{r} \ln\left(\frac{r_s}{r_s + r}\right), \quad (2)$$

with:

$$\rho_0 = \frac{M_{200}}{4\pi G r_s^3 (\ln(1+c) - c/(1+c))}, \quad (3)$$

using $M_{200} = 1.8 \times 10^{12} M_\odot$, $r_{200} = 200 \text{ kpc}$ and $r_s = 32 \text{ kpc}$. We have chosen these values to produce similar rotation curves, which exhibit $v_{\text{rot,max}}$ values as expected for a galaxy like the MW (even though discs and bulges are omitted). The rotation curves for the two profiles can be seen in Fig. 1. The inclusion of non-spherical components and their influence on the tidal tails will be part of a future study.

We investigate circular and elliptical orbits and the influence of the satellite's mass in circular orbits, therefore we use 4 different Plummer spheres (Plummer 1911):

$$\rho(r) = \frac{3M_{\text{pl}}}{4\pi R_{\text{pl}}^3} \left(1 + \frac{r^2}{R_{\text{pl}}^2}\right)^{-\frac{5}{2}} \quad (4)$$

with M_{pl} being the total mass and R_{pl} being the scale-length of the Plummer profile, to model the satellites whose parameters are given in Tab. 1. The relation between the values of M_{pl} and R_{pl} are chosen to have approximately the same

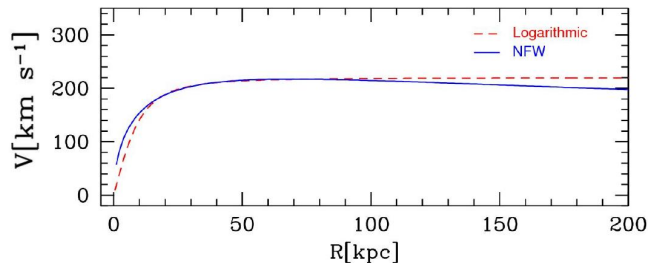


Figure 1. Rotation curves of the two potentials used to model the dark matter halo of the MW in our simulations. The red dashed line is the rotation curve of the logarithmic profile and the solid blue line is the rotation curve of the NFW profile. Note that both curves are very similar in the distance range we use to perform our simulations, in order to better compare the results.

Table 1. Description of the four different satellites used in the simulations. Column 1 is the number to identify each satellite, column 2 and 3 are the number of particles and the mass of the Plummer sphere and column 4 and 5 are the scale radius of the Plummer profile and the half mass radius of the satellite.

| | N | M_{pl} [M_\odot] | R_{pl} [kpc] | r_h [kpc] |
|---|--------|----------------------------------|--------------------------|----------------|
| 1 | 10^6 | 0.5×10^8 | 0.2 | 0.34 |
| 2 | 10^6 | 10^8 | 0.35 | 0.595 |
| 3 | 10^6 | 2×10^8 | 0.45 | 0.765 |
| 4 | 10^6 | 4×10^8 | 0.6 | 1.02 |

filling factor inside the tidal radius at a certain radius for the different satellites. The Plummer spheres are cut-off at $5R_{\text{pl}}$.

Now one can argue that, if we are using satellite galaxies, we should model their dark matter halo as well. The result would be that we would be discussing invisible dark matter tails. Instead we are using an one component model in which mass follows light. This could be identified by a satellite galaxy which has lost its outer dark matter halo already or a tidal dwarf galaxy, which was born without dark matter in the first place.

We place satellite 2 (as standard model) at 6 different distances from the centre of the galaxy according to Tab. 2 and give them velocities to produce circular orbits and let them evolve for 5 Gyr in both dark matter halos.

Then we investigate the influence of eccentricity, so we keep a fixed apo-galacticon of 80 kpc and change the velocity

Table 2. Velocity of satellite 2 at five different distances from the galactic centre to get circular orbits in the logarithmic potential (second column) and NFW potential (third column).

| R [kpc] | v_{log} [km s^{-1}] | v_{NFW} [km s^{-1}] |
|--------------|--|--|
| 15 | 171.79 | 174.36 |
| 20 | 188.65 | 187.75 |
| 25 | 198.34 | 196.90 |
| 30 | 204.27 | 203.34 |
| 35 | 208.11 | 207.93 |
| 50 | 218.43 | 214.66 |

Table 3. Eccentricity of the orbit, velocity of the satellite at apogalacticon (80 kpc) and peri-galactic distance for the eccentric orbits used in this study.

| e | v_{apo} [km s $^{-1}$] | r_{peri} [kpc] |
|-----|-------------------------------------|----------------------------|
| 0.1 | 195.64 | 65.45 |
| 0.2 | 174.21 | 53.33 |
| 0.3 | 153.07 | 43.08 |
| 0.4 | 132.05 | 34.29 |
| 0.5 | 110.96 | 26.67 |
| 0.8 | 45.21 | 8.89 |

of the satellite 2 according to Tab. 3 to produce elliptical orbits with eccentricities between 0.1 and 0.8.

Finally, we investigate the influence of the satellite’s mass using the logarithmic halo only and satellites with a mass of 0.5, 1.0, 2.0 and $4.0 \times 10^8 M_{\odot}$ orbiting at 25 kpc for 5 Gyr.

3 ANALYSIS

To analyse the tidal tails we use a code developed by V  jar (2013). This code divides both tails into bins of equal size and counts the number of stars in each bin. The size of each bin is given by the maximum length of tails that we want to analyse (L) and the number of bins we want to use (N_{bin}), therefore each bin will have a size equal to $L_{\text{bin}} = L/N_{\text{bin}}$. To count the number of stars in each bin, the code finds the centre of density of the satellite at each time-step from an output file of SUPERBOX containing this information. Then the code calculates the angular position of the satellite’s centre of density and the angular position of each star with respect to the x -axis, where the reference frame is centered on the center of the galactic potential and the initial position of the satellite is on the x -axis. Then an array containing this information for each particle is sorted by its angular position. The code puts the centre of the first bin in the centre of density of the satellite and calculates the distance between the particles and the centre of the bin using the law of cosines. If the distance is smaller than half the size of the bin, then the particle is counted in that bin.

To find a suitable place where to put the centre of the next bin the code calculates the average positions \hat{x} , \hat{y} and \hat{z} of the particles outside the bin. Then the distance \hat{r} between the centre of the previous bin and the average position of the particles outside the bin is calculated using the Pythagoras Theorem. If $\hat{r}/L_{\text{bin}} = 1$ then we have a place to set the centre of the next bin. This procedure is done until the code reaches the maximum length L defined by the user as we can see in Fig. 2.

Once we have the data of the number of particles in each bin along both tails we find that some bins have a number of particles larger than the average, this are the bins where the over-densities are located. However, identifying over-densities only by the number of particles is not very accurate, so we use another criterion. To detect over-densities properly we pick pieces of 10 kpc of tails and calculate the average number of particles in each bin inside those 10 kpc, then we detect an over-density by selecting the bins

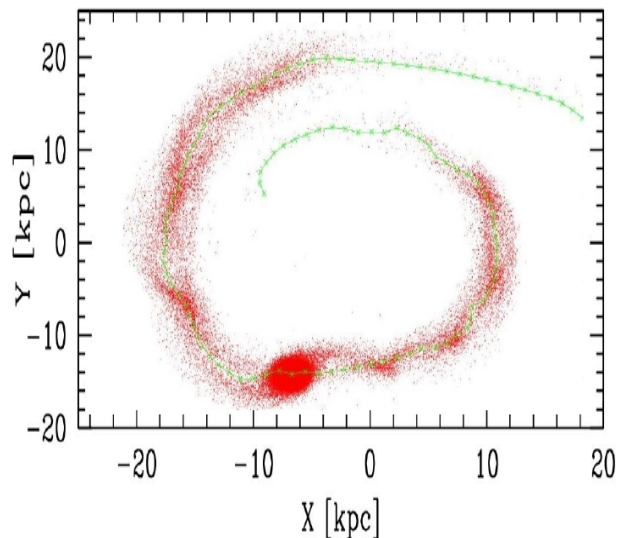


Figure 2. Path followed by the code (green line) to analyse tidal tails produced in a satellite orbiting at 15 kpc from the galactic centre

where the number of particles is larger than the average. By doing this we have the information of the distance to each bin which carries an over-density of stars. Usually there are several bins in an over-density, therefore, to measure the distance to an over-density we take the distance to the bin which is in the centre of the over-density. We also define the size of an over-density as the distance to the last bin in the over-density minus the distance to the first bin in the over-density.

As the measurements of distance and size depends on the size of the bins, used to analyse the tails, we measure this quantities using bins of 0.4 kpc, 0.5 kpc and 0.6 kpc and take the mean value in each case, then we can also calculate the error. The results of our simulations show that by choosing smaller bin-sizes, the results become unreliable because of low number statistics and larger bin-sizes will smear out the features.

After counting stars in each bin at each time-step, the code presents the information in a colour density plot, in the x -axis is the time in intervals of the time-step chosen for the output of the simulation data (10 Myr in our case) in the y -axis it shows the longitudinal separation: at the centre (0 kpc) is the satellite, at positive distances is the leading arm and negative distances represent the trailing arm. The colour scheme represents the logarithmic number densities of the tails.

We can see two different evolutionary stages of satellite 2 orbiting at 25 kpc from the Galactic Centre in the cored halo in Figure 3. After using the analysing code described in Sect. 3 we obtain the colour plot shown in the bottom panel. We clearly see how the tails grow with time. Furthermore, we see as yellow horizontal lines the over-densities which develop with time and which stay at constant distances to the satellite with time (on circular orbits).

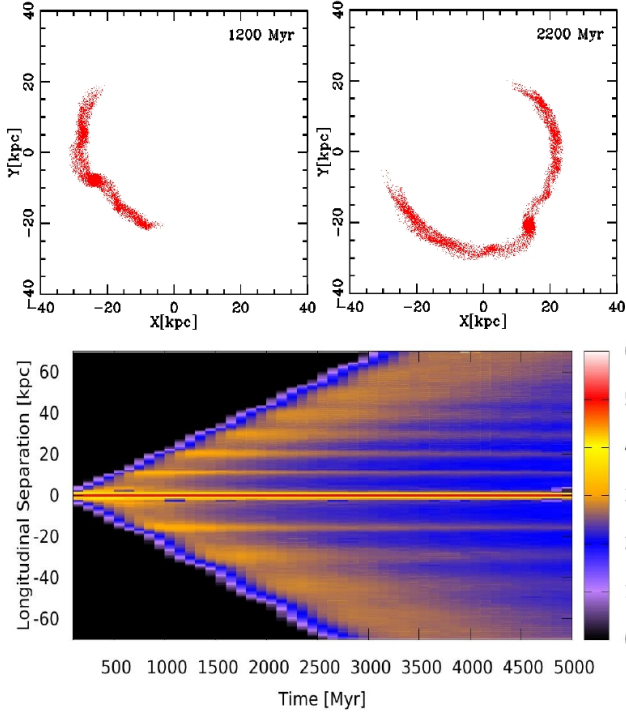


Figure 3. Lower panel: Colour density plot of the number of stars along the tails for a dSph orbiting a logarithmic dark matter halo for 5 Gyr on a circular orbit in intervals of 100 Myr. The colour bar shows the logarithm of the particles per bin. Particles in the leading arm are assigned positive distances whereas particles in trailing arm have negative distances. In the top left panel we have the satellite and its tidal tails at 1.2 Gyr and in the right panel the same satellite at 2.2 Gyr.

4 RESULTS

Once we have the data of the position and time of formation of over-densities we can compare our results with the expected values from the theory.

According to Küpper et al. (2008) the equations of motion for a particle that escapes from the tidal radius of a satellite with small velocity with respect to the satellite are given by:

$$x = \frac{4\Omega^2}{\kappa^2} x_L + \left(1 - \frac{4\Omega^2}{\kappa^2}\right) x_L \cos \kappa t, \quad (5)$$

$$y = -\frac{2\Omega}{\kappa} \left(1 - \frac{4\Omega^2}{\kappa^2}\right) x_L (\sin \kappa t - \kappa t), \quad (6)$$

$$z = 0. \quad (7)$$

With the reference frame in the centre of the satellite, the x -axis points towards the Galactic anti-centre and the y -axis points in the direction of the motion of the satellite. κ is the epicyclic frequency, Ω is the angular velocity of the satellite and x_L is the tidal radius of the satellite which we calculate according to Eq. 8, r is the radius of the orbit, M is the mass of the satellite and $M(r)$ is the mass of the halo

enclosed inside a radius r . κ is calculated according to Eq. 9:

$$x_L = r \left(\frac{M}{3M(r)} \right)^{1/3}, \quad (8)$$

$$\kappa^2 = \frac{\partial^2 \Phi}{\partial r^2} + 3\Omega^2. \quad (9)$$

If we assume a point-mass potential for the galaxy, then $\kappa = \Omega$. These equations are based on the standard potential- and epicyclic- theories (see e.g. Binney & Tremaine 2008).

Escaped particles start to de-accelerate at the turnaround points of their epicyclic orbits, i.e. when they perform a complete oscillation of 2π at $t = t_{cp} = 2\pi/\kappa$ therefore if many particles escape from the satellite and decelerate at the same position, we will see an over-density of stars at a distance $y(t_c) = y_{cp} = 12\pi x_L$ from the centre of the satellite.

The predicted values of $t_{c,p}$ and $y_{c,p}$ from the point mass-approximation as well as if we use the real potential from our simulations t_c and y_c are presented in Tabs. 4 & 5 along with the values obtained from our simulations (t_s and y_s).

If we do not assume a point-mass galaxy, then we need to solve Eq. 6 for $t = t_c = 2\pi/\kappa$. Therefore the position of the first over-density along the y -axis and the time at which is formed are given by:

$$y_c = \frac{4\pi\Omega}{\kappa} \left(1 - \frac{4\Omega^2}{\kappa^2}\right) x_L, \quad (10)$$

$$t_c = \frac{2\pi}{\kappa}. \quad (11)$$

We are analysing the simulations using satellite 2 on circular orbits at different distances from the galaxy in both analytic potentials with respect to the location and formation time of the first over-density and compare our results with the prediction formulas derived above. The values are displayed in Tabs. 4 and 5.

Using the point-mass approximation the time of formation of the first over-density is over-predicted by a factor of $\approx 1.2 \pm 0.1$. If we use the equations for the real potential the situation reverses and we under-predict the time of formation by a factor of $\approx 0.7 \pm 0.1$. This is true irrespective of the potential (logarithmic or NFW) we are using.

A similar picture presents the predictions for the location (i.e. distance) of the first over-density. Again the point-mass approximation over-predicts the location, now by a factor ranging between 6.6 and 3.6 with a decline roughly $\propto 1/r$. The full equations again deliver an under-prediction of the simulation values ranging from 0.58 and 0.75. Again we see a $1/r$ dependence of the results, i.e. the further away we are from the centre of the galaxy the closer simulation values and their respective predictions get.

We conclude that the point-mass approximation is not suitable to predict simulation results using more realistic galactic potentials. That the predictions for the formation time, using the real potential, are somewhat smaller than the measured values can be explained that the theory gives the time when the first stars reach the point of the over-density and we need some time more to establish a detectable signal (i.e. over-density). This was already pointed out in Küpper et al. (2008).

For the mismatch of the position one could imagine that it is caused by the more extended object we are using in this study and that the Lagrangian points of escape are no

Table 4. Predicted values of distance and time of formation of the first over-density for leading arm according to the theory of Küpper et al. (2008) for a point-mass galactic potential ($t_{c,p}$ & $y_{c,p}$) (columns 2 & 3), assuming a Logarithmic MW potential (t_c & y_c) (columns 4 & 5), the time of formation and position of the first over-density from our logarithmic halo simulations t_s and y_s (columns 6 & 7).

| D (kpc) | $t_{c,p}$ [Myr] | $y_{c,p}$ [kpc] | t_c [Myr] | y_c [kpc] | t_s [Myr] | y_s [kpc] |
|--------------|--------------------|--------------------|----------------|----------------|----------------|--------------------|
| 15 | 536.798 | 38.961 | 322 | 3.416 | 477 ± 24 | 5.863 ± 0.285 |
| 20 | 651.774 | 44.342 | 410 | 5.403 | 580 ± 10 | 8.620 ± 0.430 |
| 25 | 774.927 | 49.765 | 503 | 7.369 | 647 ± 38 | 11.301 ± 0.133 |
| 30 | 902.917 | 55.104 | 599 | 9.224 | 760 ± 26 | 13.700 ± 0.254 |
| 35 | 1033.950 | 60.314 | 695 | 10.949 | 883 ± 18 | 15.839 ± 0.299 |
| 50 | 1436.906 | 75.111 | 989 | 15.460 | 1243 ± 27 | 20.610 ± 0.359 |

Table 5. Predicted values of distance and time of formation of the first over-density for leading arm according to the theory of Küpper et al. (2008) for a point-mass galactic potential ($t_{c,p}$ & $y_{c,p}$) (columns 2 & 3), assuming a NFW MW potential (t_c & y_c) (columns 4 & 5), the time of formation and position of the first over-density from our NFW simulations t_s and y_s (columns 6 & 7).

| D (kpc) | $t_{c,p}$ [Myr] | $y_{c,p}$ [kpc] | t_c [Myr] | y_c [kpc] | t_s [Myr] | y_s [kpc] |
|--------------|--------------------|--------------------|----------------|----------------|----------------|--------------------|
| 15 | 528.896 | 38.577 | 331 | 4.517 | 450 ± 10 | 7.196 ± 0.323 |
| 20 | 654.910 | 44.484 | 417 | 5.872 | 543 ± 15 | 9.974 ± 0.110 |
| 25 | 780.564 | 50.006 | 505 | 7.293 | 623 ± 38 | 11.484 ± 0.084 |
| 30 | 907.017 | 55.271 | 596 | 8.772 | 763 ± 18 | 13.524 ± 0.093 |
| 35 | 1034.834 | 60.349 | 688 | 10.302 | 900 ± 15 | 15.619 ± 0.297 |
| 50 | 1428.756 | 74.827 | 981 | 15.144 | 1277 ± 38 | 20.270 ± 0.407 |

longer almost coinciding with the distance of the orbit, i.e. that $\Delta r = r \pm x_L$ is not negligible any longer. But this would mean that we see over- and under-predictions depending if we analyse the leading or the trailing arm of our object. This is not the case in our simulations. We only detect a smaller deviation for the leading arm than for the trailing arm but both directed in the same direction with respect to over- and under-predictions. We suspect that the zero velocity assumption (i.e. that stars leave the satellite with small velocities only) is no longer valid for the extended objects we use.

The discrepancy between the point-mass approximation and the real simulation values was not visible in the results of Küpper et al. (2008), as they were actually using a point-mass potential to mimic the galaxy together with the point-mass approximation to compare their results. In that sense we agree with Küpper et al. (2008), just one has to use the prediction equations matching the used potential.

After comparing the theory with our simulations, we analyse the rate of growth of the tails arising from the satellites. As the growth of the tails is linear with time for satellites on circular orbits, we simply take two values of the length of the tails together with 2 values of time and calculate the slope. We use the length at 3000 Myr and the length at 0 Myr, which is zero to calculate the growth-rate. For satellites orbiting on eccentric orbits, the growth of the tails is not linear with time, tails are stretched and compressed as the satellite passes through peri- and apo-galacticon, respectively. To measure the rate of growth we have taken the values for the length of the tails between the time after two consecutive peri-centre passages measured half-way to the next apo-galacticon.

We find that the trailing arm always grows faster than the leading arm irrespective of circular or elliptical orbits

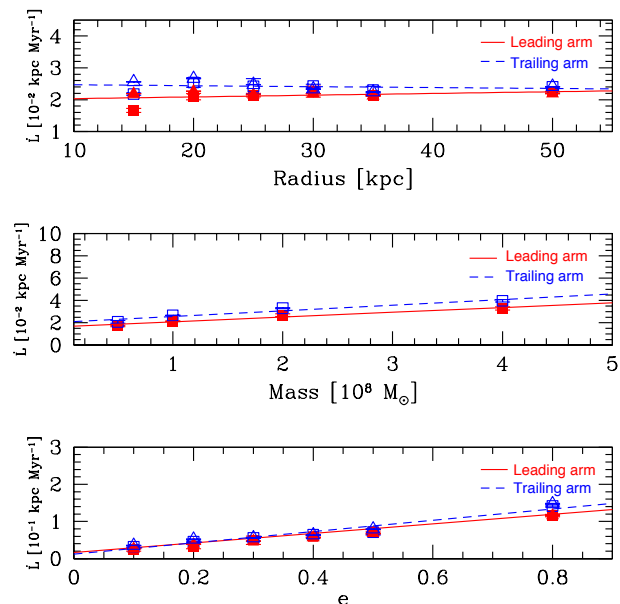


Figure 4. Rates of growth of leading and trailing arm depending on the radius of circular orbits (top) the mass of the satellite (middle) and the eccentricity of the orbit (bottom). We plot data from simulations using a logarithmic halo as squares and a NFW profile as triangles. Red filled symbols are data from the leading arm and blue open symbols are data from the trailing arm. Red and blue lines are the best linear fits for leading and trailing arm respectively. As we see no difference between the logarithmic and NFW halo results we fit both results simultaneously. The exception is the middle panel as for varying satellite mass we only used the logarithmic potential.

(see Fig. 4). For circular orbits, the rates of growth are independent of the radius of the orbit and ~ 0.02 kpc Myr $^{-1}$ for leading arms and ~ 0.025 kpc Myr $^{-1}$ for trailing arms as shown in the top panel of Fig. 4. One can also see that these results are independent of the form of the potential, i.e. using a logarithmic or a NFW halo.

This result shows that for the growth of the tidal tails, the underlying potential is of no importance. The velocity of the tail growth is given by the parameters of the satellite only. The fact that the trailing arm is growing slightly faster can be understood by the fact that stars are leaving with similar velocities through the Lagrangian points. For an extended object as used in our simulations, those stars have slightly different angular velocities compared to that of a circular orbit at this distance. These differences could differ in magnitude for the leading and trailing arm leading to this asymmetry of tail growth.

In the middle panel of Fig. 4 we see clearly that the growth depends on the mass of the satellite in a linear fashion. The rate of growth for the the leading arm varies from 0.0172 ± 0.0004 kpc Myr $^{-1}$ for a satellite of $0.5 \times 10^8 M_{\odot}$ up to 0.0329 ± 0.0009 kpc Myr $^{-1}$ for a satellite of $4.0 \times 10^8 M_{\odot}$. The best linear fits are given by the Eq. 12 for the leading arm and Eq. 13 for the trailing arm:

$$\dot{L}_L = 0.0043 \pm 0.0007 \times M + 0.017 \pm 0.002, \quad (12)$$

$$\dot{L}_T = 0.0051 \pm 0.0010 \times M + 0.021 \pm 0.002. \quad (13)$$

For these simulations we have only used the logarithmic potential as galactic potential.

Here we clearly see the dependence on the internal satellite parameters. Stars leaving the satellite should have escape velocity or slightly higher. We conclude that the assumption that stars leave the satellite with zero or negligible relative velocity may be valid for small star clusters but not for very massive and extended objects. In this respect our study shows a disagreement with the assessment of Küpper et al. (2008).

Finally, we find that the rate of growth of the tails measured between peri-galacticon and the next apo-galacticon for satellites orbiting in eccentric orbits seems to depend linearly on the eccentricity of the orbit and varies from 0.0241 ± 0.0022 kpc Myr $^{-1}$ for the leading and 0.0320 ± 0.0013 for trailing arm for an eccentricity of 0.1, up to 0.1157 ± 0.0019 and 0.1474 ± 0.0063 kpc Myr $^{-1}$ for leading and trailing arm, respectively, for an eccentricity of 0.8.

The best linear fits are shown in Eq. 14 for the rate of growth of the leading arm and in Eq. 15 for the rate of growth of the trailing arm.

$$\dot{L}_L = 0.128 \pm 0.005 \times e + 0.010 \pm 0.002, \quad (14)$$

$$\dot{L}_T = 0.152 \pm 0.013 \times e + 0.012 \pm 0.006. \quad (15)$$

In our simulations this is explained easily. The higher the eccentricity the deeper into the galactic potential the satellite is orbiting. Stars get lost by tidal shocks at peri-galacticon passages. The closer to the galactic centre the satellite is orbiting the smaller the instantaneous tidal radius will be and the more stars can get stripped, which have higher relative velocities with respect to the satellite. Again here we see a clear deviation from the zero velocity assumption.

In Fig. 5 we show the distance to the first over-density in the leading and the trailing arm. We find that the distance

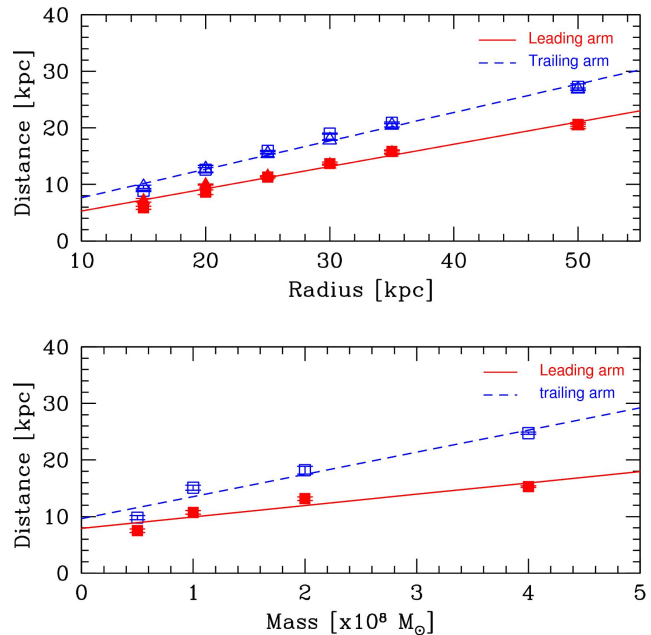


Figure 5. Top panel: Distance to the first over-density in leading and trailing arms as function of the radius of the orbit. Bottom panel: Distance to the first over-density as function of the satellite mass. We plot data from simulations using a logarithmic halo as squares and a NFW profile as triangles. Red filled symbols are data from the leading arm and blue open symbols are data from the trailing arm. Red and blue lines are the best linear fits for leading and trailing arm respectively. As we see no difference between the logarithmic and NFW halo results we fit both results simultaneously. Again in the lower panel we only show simulations using the logarithmic halo for the varying satellite mass.

to the first over-density in leading and trailing arm depends on the radius of the orbit and the mass of the satellite as expected from the theory of Küpper et al. (2008) but does not depend on the potential used to model the MW. This can be seen in the top panel as the symbols for the logarithmic halo and the NFW profile basically overlap.

We also find that in the leading arm the first over-density is always at a smaller distance from the satellite than in the trailing arm. After the formation of the over-densities, the distance to them remains constant (see example in Fig. 3).

The difference in the distance between the two tails is a puzzling detail of our simulations. It could be explained by the fact that we have a much more extended object than used in the previous study. Again, the difference in distance between the two Lagrangian points should be taken into account. But, then we would expect that this difference is more pronounced the closer we are to the centre of the galaxy. That we see the opposite trend in our results is therefore counter-intuitive and needs further investigation. Nevertheless, it is a fact which should be taken into account when analysing observational results. The fact that tidal tails of one and the same object have not same length and that the over-densities appear at different locations is not necessarily a sign for an interaction with another object.

We have studied the distance to the first over-density in the leading and trailing arm. In reality, we have measured the distance to the centre of the over-density, because the

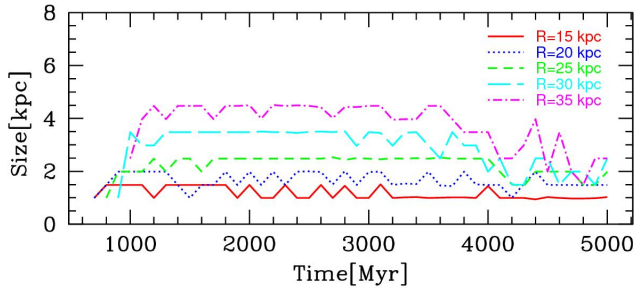


Figure 6. Size of the first over-density as function of time for a satellite orbiting at 15 kpc (solid red line), 20 kpc (blue dotted line), 25 kpc (green short dashed line), 30 kpc (cyan long dashed line) and 35 kpc (magenta dot dashed line). We can note that after ~ 3600 Myr the size of the over-density is decreasing down to about 2 kpc.

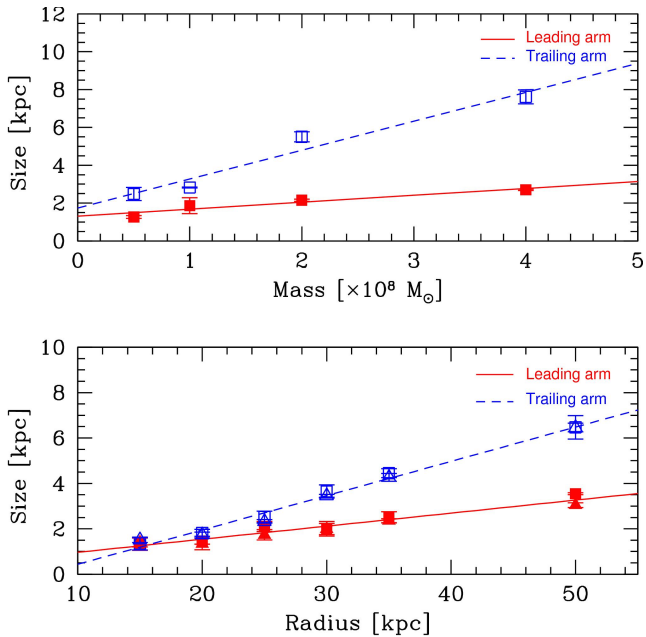


Figure 7. Size of the first over-density as function of the mass of the satellite (top panel). In the lower panel we plot the size of the first over-density as function of the radius of the orbit. We plot data from simulations using a logarithmic halo as squares and a NFW profile as triangles. Red filled symbols are data from the leading arm and blue open symbols are data from the trailing arm. Red and blue lines are the best linear fits for leading and trailing arm respectively. As we see no difference between the logarithmic and NFW halo results we fit both results simultaneously. Again in the top panel we only show simulations using the logarithmic halo for the varying satellite mass.

over-densities have a size. We calculate the mean value of all bins which present the over-density. As the size of these over-densities may help us to distinguish further between Galactic and/or satellite properties, we now take a closer look at the sizes.

We find that after the formation of the over-densities they have a nearly constant size, however, the size is decreasing after ~ 3600 Myr as we can see in Fig. 6

To study how the size depends on the properties of the satellite we take an average of the size of the over-densities

between 1 and 3 Gyr, i.e., a time-span, starting after the formation of the over-densities, where the size of them does not vary significantly. The results are shown in Fig. 7.

We find that the size of the first over-density in the leading arm depends only weakly on the radius of the orbit and does not depend on the potential used to model the MW. The size varies from 1.33 ± 0.16 kpc for a satellite orbiting at 15 kpc up to 3.55 ± 0.05 kpc for a satellite orbiting at 50 kpc. In the trailing arm we see a clear dependence of the size of the first over-density with the radius of the orbit. The size of the first over-density increases with increasing radius of the orbit from 1.35 ± 0.16 kpc for a circular orbit at 15 kpc up to 6.47 ± 0.30 kpc for a circular orbit at 50 kpc.

The size of the first over-density depends on the mass of the satellite. In the trailing arm the size of the first over-density increases from 2.49 ± 0.20 kpc for a satellite with a mass of $0.5 \times 10^8 M_\odot$ up to 7.62 ± 0.22 kpc for a satellite with a mass of $4.0 \times 10^8 M_\odot$. In the leading arm, the size of the first over-density depends only weakly on the mass of the satellite ranging from 1.27 ± 0.04 kpc for a satellite with a mass of $0.5 \times 10^8 M_\odot$ up to 2.71 ± 0.02 kpc for a satellite with a mass of $4.0 \times 10^8 M_\odot$. Apparently, the size of the first over-density in leading arms depends linearly with the mass of the satellite, however, for trailing arms it could be a power law. We show in Fig. 7 the best linear fits to the data of the size of the first over-density in the leading arm and trailing arm depending on the radius of the orbit in kpc (Eq. 16 and Eq. 17) and the Mass of the satellite in M_\odot (Eq. 18 and Eq. 19):

$$S_L = 0.058 \pm 0.005 \times r + 0.4 \pm 0.1, \quad (16)$$

$$S_T = 0.15 \pm 0.01 \times r - 1.1 \pm 0.2. \quad (17)$$

$$S_L = 0.37 \pm 0.08 \times M + 1.3 \pm 0.2, \quad (18)$$

$$S_T = 1.5 \pm 0.2 \times M + 1.7 \pm 0.5. \quad (19)$$

Again we see a clear asymmetry of the two tails. The size of the first over-density in the trailing arm grows about three times faster with mass and distance than the one of the leading arm. This cannot be explained by the use of an extended object alone. Even though we do not have a valid explanation for this finding, it is a fact which should be taken into account when observing real objects.

Finally, we combine the data from the distance to the first over-density in the leading and trailing arms with the size of the first over-density for simulations of satellites orbiting a logarithmic halo in circular orbits. The data is shown in Fig. 8. The reason for this exercise is that in this way we might be able to distinguish between internal and external effects, i.e. mass of the satellite and the potential strength. Unluckily, we do not see such a trend in Fig. 8 as all data-points follow the same relation, no matter the mass of the satellite or the distance to the galaxy.

Nevertheless, we can establish a relation between the distance to the first over-density and the size of the first over-density for leading and trailing arms separately, which could be observationally investigated. A simple linear fit to the data from our simulations gives the following relations:

$$S_L = 0.15 \pm 0.01 \times D + 0.2 \pm 0.2, \quad (20)$$

$$S_T = 0.31 \pm 0.04 \times D - 1.7 \pm 0.6. \quad (21)$$

Here, S_L is the size of the first over-density in leading arm and S_T is the size of the first over-density in trailing arm

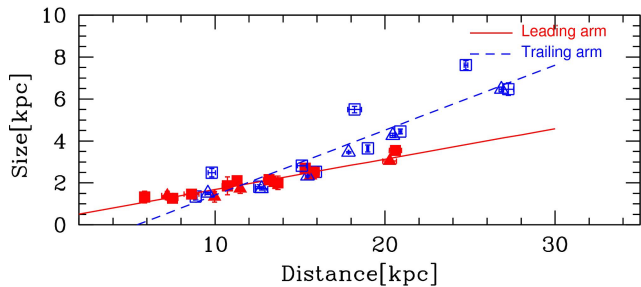


Figure 8. Size of the first over-density as function of the distance to the first over-density for trailing arms (blue symbols) and leading arms (red symbols) using simulations of a satellite orbiting a logarithmic halo on circular orbits and the best linear fits in red for the leading and blue for the trailing arm.

and D is the distance (in kpc) to the over-density from the centre of the satellite.

5 DISCUSSION AND CONCLUSIONS

From simulations of dwarf galaxies orbiting a spherical logarithmic and a NFW dark matter halo (instead of a point mass potential) we find that the theory of Küpper et al. (2008), giving theoretical estimates for the time of formation and the distance to the first over-densities in tidal tails is over-predicting the results we are obtaining with our simulations. In case of the location of the first over-density this can be up to factor of six. We have shown that this is not due to the fact of the different sized objects the two studies use but that Küpper et al. (2008) were right with their estimates as they also used a point-mass potential in their simulations. The solution is that one cannot use the simple equations from their study but has to go back and solve the original epicyclic equations for the potential one actually uses. We still see some discrepancies but those could be explained by the real setup in contrast to an idealised, approximated theoretical frame-work. In that respect we verify the results of Küpper et al. (2008).

In our study we have shown that the growth-rate of tidal tails (on circular orbits) does not depend on the potential strength of the galactic potential as the tails grow with the same rate independent of the potential used (logarithmic halo or NFW halo) and distance to the centre of the galaxy. The tails grow faster if the satellite is more massive. We conclude that this is because the simple zero velocity approximation for the epicyclic equations is in fact not completely valid. In reality in larger, more massive objects stars escape with higher relative velocities.

This can be seen as well, when we investigate the growth-rate as function of the eccentricity of the orbit. The further in an object orbits, the stronger is the decrease of the tidal radius at peri-centre. Therefore, more stars are able to leave the satellite and escape into the tails. Naturally, these stars have higher relative velocities and therefore we grow tidal tails faster when we orbit with higher eccentricity.

Even though we could calculate the rates of growth for both tails, using eccentric orbits, we do not have sufficient data of the over-densities, because the code of Vejar (2013) does not consider the possibility of having more than 2 tidal

tails, a feature which occurs naturally if new stars are lost at peri-galacticon. The new and old tails will align with each other when the satellite is approaching apo-galacticon.

We find a relation between the distance to the first over-density in the leading and trailing arms and the radius of the orbit and/or the mass of the satellite. As the rate of growth does not depend on the radius of the orbit we conclude that the relation between the distance of the first over-density and the radius of the orbit must be due to the change in the tidal radius alone. This is verified when only changing the mass of the satellite at the same distance to the galaxy. A change in the epicyclic frequency κ and the angular velocity Ω in affecting the results cannot be excluded but are of secondary order.

A very particular result of our study is the visible asymmetry between the leading and the trailing arm, with the trailing arm growing faster and being larger than the leading arm. The most obvious explanation would be the difference in distance between the two Lagrangian points in large objects as used in our study. This is of course an effect which plays a role but it cannot explain why this trend is more pronounced at larger radii from the galaxy, where this difference should become more insignificant.

Furthermore, we find a relation between the size of the first over-density and the radius of the orbit or the mass of the satellite. This relation is very clear for trailing arms but not as clear for leading arms, where the size of the first over-density is very close to 2 kpc in all simulations. A possible explanation for this behaviour is that particles not always escape with the same velocity from the satellite but around a central value v_{esc} and with a small velocity dispersion σ . According to the theory of Küpper et al. (2008) this spread in the escape velocity will lead to a spread in the value of y_c at which the particles turn around. Therefore, we will have an extended over-density with a size S . We expect that satellites with higher masses produce larger σ values and therefore larger over-densities. Why this is so strongly visible in trailing arms only is a study on its own and should be dealt with in a future investigation.

The dependency with the radius is similar. The sizes of over-densities in the trailing arms grows about three times faster than the respective size in the leading arm. Again this obvious asymmetry is not easy to explain and deserves further studies.

Finally, we combine the results of distance and size of the over-densities and find a single linear relation between the distance to the first over-density and its size for leading and trailing arms separately but independent of the mass of the satellite, the radius of the orbit and its eccentricity. This relation could be investigated with detailed observations of tidal tails.

Acknowledgments: MF acknowledges financial support of Fondecyt grant No. 1130521, Conicyt PII20150171 and BASAL PFB-06/2007. BR acknowledges funding through Fondecyt grant No. 1161247. BR thanks A. Alarcon Jara and D.R. Matus Carrillo for their help with the code SUPERBOX and useful discussions during the realization of this work.

REFERENCES

- Belokurov, V. et al. 2006, ApJ, 642, L137
- Binney, J., Tremaine, S. 2008, 'Galactic Dynamics' 2nd edition, Princeton University Press, ISBN: 9780691130279
- De Blok, W.J.G., and Bosma, A. 2002, A&A, 385, 816
- Fellhauer, M., Kroupa, P., Baumgardt, H., Bien, R., Boily, C.M., Spurzem, R., Wassmer, N. 2000, New Ast., 5, 305
- Fellhauer, M., Belokurov, V., Evans, N.W., Wilkinson, M.I., Zucker, D.B., Gilmore, G., Irwin, M.J., Bramich, D.M., Vidrih, S., Wyse, R.F.G., Beers, T.C., and Brinkmann, J. 2006, ApJ, 651, 167
- Koposov, S., Rix, H.-W., and Hogg, W. 2010, ApJ, 712, 260
- Küpper, A., Macleod, A., and Heggie, D. 2008, MNRAS, 387, 1248
- Küpper, A., Kroupa, P., Baumgardt, H., and Heggie, D. 2010, MNRAS, 401, 105
- Küpper, A., Lane, R., and Heggie, D. 2012, MNRAS, 420, 2700
- Majewski, S., Skrutskie, M.F., Weinberg, M., Ostheimer, J. 2001, ApJ, 548, L165
- Navarro, F., Frenk, S., and White, D.M. 1996, ApJ, 462, 563
- Odenkirchen, M. et al. 2001, ApJ, 548, L165
- Plummer, H.C. 1911, MNRAS, 71, 460
- Véjar, R. 2013, Thesis(Título), Universidad de Concepción
- Vivas, K. et al. 2001, ApJ, 554, L33
- Williams, M.E.K. et al. 2011, ApJ, 782, 102